

Intermediate-velocity gas observed towards the Shajn 147 SNR

S. Sallmen¹ and B.Y. Welsh²

¹ Department of Physics, Univ. of Wisconsin - La Crosse, La Crosse, WI 54601

² Experimental Astrophysics Group, Space Sciences Laboratory, UC Berkeley, Berkeley

Received 16 January 2004 / Accepted 12 July 2004

Abstract. We present high-resolution spectra ($R \sim 3 \text{ km s}^{-1}$) of the interstellar Na I and Ca II interstellar absorption lines observed towards 3 early-type stars with distances of 360 to 1380 pc along the line-of-sight towards the 800 pc distant Shajn 147 (S147) Supernova Remnant (SNR). These data are supplemented with far-UV (912 - 1180 Å) absorption spectra of HD 36 665 and HD 37 318 recorded with the NASA Far Ultraviolet Spectroscopic Explorer (*FUSE*) satellite. The observations reveal intermediate-velocity (IV) absorption features at $V_{\text{helio}} = +92 \text{ km s}^{-1}$ towards HD 37 318 and at $V_{\text{helio}} = -65$ & -52 km s^{-1} towards HD 36 665, in addition to several other gas cloud components with lower velocity. These IV components can be associated with the expansion of the SNR that has disrupted the surrounding interstellar gas.

The IV component at $V = +92 \text{ km s}^{-1}$ seen towards HD 37 318 was detected only in the far-UV lines of Fe II and N II, suggesting that it is composed mainly of warm and ionized gas. The two IV components observed towards HD 36 665 were detected in Na I, Ca II, N I, N II, O I and Fe II, indicating that it is composed of both neutral and ionized gas shells. Highly ionized gas was detected in the O VI ($\lambda 1032 \text{ Å}$) absorption line at $V \sim +40 \text{ km s}^{-1}$ towards both stars. This hot and highly ionized gas component is characterized by a column density ratio of $N(\text{C IV})/N(\text{O VI}) < 0.27$, which is consistent with that predicted by current models of evolved SNRs. However, we cannot preclude its origin in the interstellar medium in line-of-sight to S147.

Column-density ratios of [Mg/Fe], [Al/Si],[Si/Fe], [N/Fe], [O/Fe] and [Na/Ca] have been derived for the IV gas components detected towards S147. Similar ratios have also been derived for fast-moving gas observed towards two other SNRs in order to gain some insight into the behavior of element abundances in the disturbed interstellar gas associated with these regions. In all cases except for Na and Ca, these elements appear to be present with near-solar abundance ratios.

Key words. ISM—: bubbles, supernova remnants

1. Introduction

Observations of supernova remnants (SNRs) can provide important information concerning both the energy and ionization balance of the interstellar medium (ISM), since supernova explosions and the strong stellar winds from OB stars are the dominant sources of high-temperature, high-velocity shocked gas in the ISM. The majority of the immense energy that is released in a supernova event is transferred into the kinetic energy of the gas and dust ejecta, which then subsequently interacts and changes both the physical and chemical state of the ambient interstellar gas. The spectral (emission and absorption) signatures of the disturbed low-density gas surrounding SNRs are best sampled in the ultraviolet regime, which contains spectral lines covering a wide range of ionization stages from a large variety of elements. When coupled with high spectral resolution visible observations (which provide a key diagnostic of the kinetics of the disturbed ambient interstellar gas), it is possible to present a detailed picture of the ionization state, chemical

abundance and velocity structure of the remnant's interaction with the surrounding ISM.

Recently we have been carrying out a program of absorption observations of nearby galactic SNR sight-lines using both the NASA Far Ultraviolet Spectroscopic Explorer (*FUSE*) satellite (Moos et al. 2000) and ground-based visible observations of the interstellar Na I and Ca II absorption lines. Thus far we have analyzed the absorption characteristics of the disturbed interstellar gas associated with the Monoceros Loop SNR (Welsh et al. 2001, 2002a), the Cygnus Loop SNR (Welsh et al. 2002b), the RCW 114 nebula (Welsh et al. 2003a) and the IC 443 remnant (Welsh & Sallmen 2003b). These observations have generally revealed a complex pattern of shocked neutral and ionized shells of interstellar gas surrounding these remnants, with gas cloud velocities as high as $\sim -100 \text{ km s}^{-1}$ being detected. An overabundance of the refractory elements of Fe, Si and Al has been found for all these disturbed interstellar regions, consistent with the notion that substantial dust grain sputtering has taken place within the expanding shells of gas. In contrast, the abundances of N, O and Ar derived from their lowest ionization stage are less than the total abundances of the elements found in the general

Shajn 147

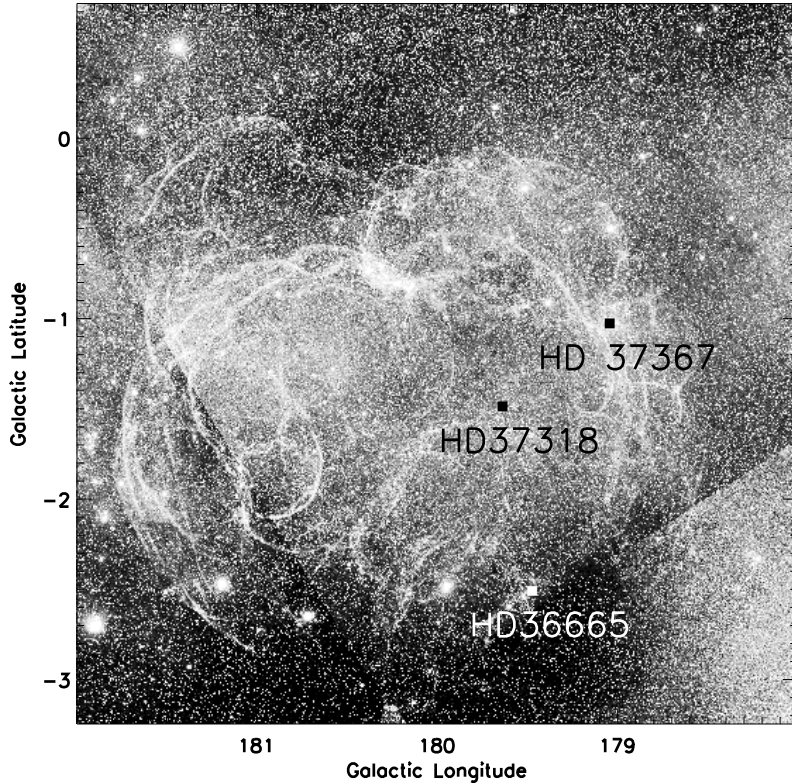


Fig. 1. Positions of the 3 stars (1) HD 36 665, (2) HD 37 318 and (3) HD 37 367 with respect to the H- α emission from the Shajn 147 SNR. The digitized Sky Survey image was taken from the SkyView web-site at <http://skyview.gsfc.nasa.gov>.

ISM, suggesting that ionization processes may be dominating the depletions inferred for the fast-moving gas (Jenkins et al. 1998). Absorption associated with the high-ionization, high-temperature O VI($\lambda 1032\text{\AA}$) ion has not been detected in the gas surrounding old ($> 30,000$ years) SNRs. However, towards the far younger Vela SNR high-velocity ($V > 100 \text{ km s}^{-1}$) absorption features have been detected in the high-ionization lines of C IV($\lambda 1550\text{\AA}$), Si IV($\lambda 1402\text{\AA}$) and O VI (Jenkins et al. 1984). In addition, *emission* observations of these high-ionization UV lines, seen in the fast shocked gas filaments of SNRs, have placed important constraints on the dynamical pressure and shock mechanisms present in these highly disturbed regions of the ISM (Sankrit et al. 2003, Sankrit & Blair 2002).

The Shajn 147 SNR ($l = 180.3^\circ$, $b = -1.7^\circ$) is an optically faint, highly filamentary galactic supernova remnant (SNR) of age $\sim 10^5$ years with a distance of $\sim 800\text{pc}$ (Kundu et al. 1980). It has a shell-like structure of diameter 3° as revealed by both radio (Furst & Reich 1986) and visible (Minkowski 1958) observations. No X-ray emission has been detected from this remnant (Sauvageot et al. 1990). Optical absorption studies of the interstellar Ca II K-line at 3933\AA observed towards the star HD 36 665 ($d \sim 880\text{pc}$) by Silk & Wallerstein (1973) revealed intermediate-velocity (IV) gas with a velocity of $\sim -69 \text{ km s}^{-1}$ that was associated with the expansion of the SNR blast wave into the surrounding ISM. Follow-up *I.U.E.* ab-

sorption studies of the sight-lines towards the stars HD 36 665 and HD 37 318 confirmed the disturbed state of the ISM surrounding Shajn 147, with absorption features being detected at respective velocities of $V_{helio} = -63 \text{ km s}^{-1}$ and $V_{helio} = +92 \text{ km s}^{-1}$ (Phillips, Gondhalekar & Blades 1981 hereafter PGB81; Phillips & Gondhalekar 1983 hereafter PG83). These IV absorption components were detected in UV lines such as C II, C II*, Al II and Fe II, but not in the high-ionization ($T \sim 80,000\text{K}$) lines of C IV or Si IV. Similarly, no IV absorption features were detected in neutral ions such as C I or N I towards either star. From these UV data it was concluded that the shocked gas surrounding the SNR is not strongly ionized, consistent with what may be expected from an evolved remnant.

In this Paper we present high spectral resolution ($R \sim 3 \text{ km s}^{-1}$) observations of the visible interstellar Na I and Ca II absorption lines seen towards 3 stars (HD 36 665, HD 37 318 and HD 37 367) with sight-lines towards Shajn 147. These data are complemented by far-ultraviolet absorption observations towards the former two stars (that have distances comparable with Shajn 147) recorded over the $912 - 1180\text{\AA}$ range using the NASA *FUSE* satellite. Our observations confirm the presence of a complex of absorption components that span a range of velocities from -65 to $+90 \text{ km s}^{-1}$, with the highest-velocity components being associated with the expansion of the SNR into the ambient interstellar medium. Our far-UV observations sug-

Table 1. Stellar Target Information

Star	(l,b)	m_v	Sp	E(B-V)	$V \sin i$ km s ⁻¹	R.V. km s ⁻¹	distance (pc)
HD 36 665	(179.5°, -2.5°)	8.2	B0Ve	0.64	60	+9.0	880
HD 37 318	(179.6°, -1.5°)	8.4	B1IV	0.61	50	+5.8	1380
HD 37 367	(179.0°, -1.0°)	6.0	B2IV	0.40	20	+29.6	361(+150,-85)*

* = *Hipparcos distance*

gest that these intermediate-velocity clouds contain both neutral and ionized gas and that the refractory elements present in these components possess near-solar abundances.

2. Observations

We have carried out visible absorption observations towards HD 36 665, HD 37 318 and the foreground star HD 37 367 using the Aurelie echelle spectrograph at the 1.52m telescope of the Observatoire de Haute Provence (France) on the nights of September 26 - 29th, 2002. Data were recorded separately at the Na I ($\lambda 5890\text{\AA}$) and Ca II ($\lambda 3933\text{\AA}$) interstellar lines. In Table 1 we list the relevant astronomical data for the 3 stars, which includes their visual magnitudes, spectral types, reddening values, rotational velocity ($V \sin i$), radial velocity (R.V.) and distance estimates. These values were taken from the on-line Simbad astronomical data-base, with the distance and reddening estimates being taken from PGB81, Savage et al. (1985) and the Hipparcos catalog (ESA 1997). For HD 36 665 and HD 37 318 we derived averaged rotational velocities from the widths of several prominent stellar lines in their visible and far-UV spectra. The spectral type for HD 36 665 was taken from Halbedel et al. (1996). The positions of the 3 targets with respect to the optical H- α emission contours of the Shajn 147 SNR are shown in Figure 1.

The photon data were recorded with an EEV 2048 x 1024 CCD detector and the raw spectral images extracted using data reduction procedures analogous to those detailed in Sfeir et al. (1999). Briefly these software programs perform cosmic ray removal, background subtraction, flat-fielding, optimal spectral order extraction and wavelength assignment (from Th-Ar calibration spectra) on the recorded data. The resolution of the resultant spectra was 2.75 km s^{-1} and the wavelength accuracy of the calibrated data was $\sim \pm 0.02 \text{ \AA}$. The S/N ratio (per pixel) of the recorded spectra were $\sim 30:1$ for the Na I spectra and $\sim 20:1$ for the Ca II data. All velocities subsequently quoted in this Paper are reported in the heliocentric frame of reference. Finally, we have removed the many telluric water vapor absorption lines that particularly affect contamination of the Na I D-line-profiles using a computed synthetic atmospheric scaled transmission spectrum as described in Lallement et al. (1993).

The *FUSE* spectra of HD 36 665 and HD 37 318 were taken using the LWRS (30 x 30 arc second) spectrograph aperture, with the data being recorded in the detector time-tag mode. Photon events were recorded for a total exposure time of 26 ksec for HD 36 665 and 35 ksec for HD 37 318. The data were processed using version CFv2.2.3 of the *FUSE* science data reduction (CALFUSE) pipeline, which corrects for geometri-

cal image distortions, background subtraction, image thermal drifts, detector deadtime and wavelength calibration (Sahnou et al. 2000). Due to the relatively high reddening of both objects, the far-UV spectra at wavelengths $< 1000\text{\AA}$ were of a low S/N ratio ($< 5:1$), whereas the spectra were better exposed at longer wavelengths. Therefore, only the data contained in the LiF1a and LiF1b spectral channels (i.e. $\lambda > 1000\text{\AA}$) have been utilized in this analysis. Since the *FUSE* instrument does not provide absolute wavelength accuracies to better than $\pm 20 \text{ km s}^{-1}$, we have determined the far-UV wavelength scale with reference to the many H₂ molecular lines that were detected in these UV spectra. We have assumed that these lines are formed at the same (heliocentric) velocity as that of the main absorption component detected in the Na I interstellar D-lines at $V_{helio} = +14.5 \text{ km s}^{-1}$ for HD 36 665 and at $V_{helio} = +12.0 \text{ km s}^{-1}$ for HD 37 318 (see Table 2). We estimate that the accuracy of our derived far-UV wavelengths is $\sim \pm 5 \text{ km s}^{-1}$. The resolution of the LiF channel data used in the subsequent analysis was found to be $R \sim 21,000$ (i.e. 14 km s^{-1}), as determined from fitting several weak interstellar absorption lines in the 1020 - 1180 \AA wavelength region.

3. Interstellar Analysis

We have determined the local stellar continua for the interstellar Na I and Ca II absorption lines for the 3 stars using a multi-order polynomial. Errors associated with this placement are automatically generated by the software routine and have been discussed in Welsh et al. (1990). For these visible interstellar lines the local continua were well-behaved and the placement error was small. The resultant residual intensity profiles are shown in Figures 2 and 3. These profiles were then fit with multiple absorption components (identified with interstellar gas ‘clouds’) using a line-fitting program described in Sfeir et al. (1999). This program assigns a 3-parameter theoretical fit to the observed absorption profiles by assigning values for the interstellar gas cloud component velocity, V , a gaussian velocity dispersion, b and a cloud component column density, N . This fitting procedure works very well for absorption components that are not saturated, but the process leads to large uncertainties in the derived column densities for the central cores of spectral lines that possess very high values of saturation. In such cases (i.e. for the central line-core components) the best-fit values of b and N shown in Table 2 (and marked with *) are not well constrained and are listed only for the purpose of showing the velocity range over which the central absorption occurs. Fortunately, most of the IV absorption components located far from the saturated line-cores are unsaturated and reli-

Table 2. Na I and Ca II Absorption Line Best-Fit Parameters (stars listed by increasing distance)

Star	V km s ⁻¹	<i>b</i>	N (10 ¹⁰ cm ⁻²)		V km s ⁻¹	<i>b</i>	N (10 ¹⁰ cm ⁻²)	Na I/Ca II
HD 37 367								
...Na I...				...Ca II...	+1.3	4.4	19±3	-
	+13.5	3.6	620±30		+16.7	6.0	125±30	5.0
					+22.0	3.8	85±20	-
					+31.5	7.9	41±15	-
HD 36 665								
...Na I...	-67.0	4.1	7.6±0.5	...Ca II...	-66	3.8	90±30	0.084
					-56.0	7.5	72±23	-
					-48.0	8.0	44±12	-
					-34.0	2.7	14±4	-
					-6.0	4.8	55±12	-
	+2.8	3.6	190±35		+6.0	4.9	150±25	-
	+14.5	4.7	>1350*		+17.5	7.0	380±40	>3.6
	+34.0	0.8	6.9±1		+30.0	3.0	55±20	0.13
	+39.5	2.1	2.2±0.5		+36.0	4.8	45.0±8	0.049
HD 37 318								
...Na I...	-35.5	4.0	4.6±1.0	...Ca II...	-33.0	2.2	6.6±2.0	0.7
	+12.0	5.7	>2500*		+13.0	6.4	205±40	>120
	+24.5	2.6	55±10		+21.0	7.4	290±50	-
	+37.0	3.8	7.9±1.5				<3.0	<2.6

* = saturated component

Table 3. Best-Fit Parameters to the IV components of the far-UV absorption lines

Line	V km s ⁻¹	<i>b</i>	N (10 ¹² cm ⁻²)	V km s ⁻¹	<i>b</i>	N (10 ¹² cm ⁻²)
HD 36 665						
...Fe II 1144.9Å...	-65	9.0	33±6	-48	9.2	23±8
...Fe II 1122.0Å...	-64	9.0	33±6	-55	9.2	23±8
...N I 1135.0Å...	-64	6.7	76±20	-51	5.4	24±5
...N I 1134.2Å...	-63	6.7	76±20	-49	5.4	24±5
...N II 1084.0Å...				-53	18.0	240±30*
...O I 1039.2Å...	-65	5.4	270±50	-56	4.2	330±80
...O VI 1031.9Å...	+10	17.5	185±40	+45	9.0	36±5
HD 37 318						
...Fe II 1144.9Å...				+92	3.7	40±7
...Fe II 1122.0Å...				+90	4.2	40±7
...N II 1084.0Å...				+92	16.2	155±20*
...O VI 1031.9Å...	+11.0	9.5	55±5	+38	19.0	33±10

* = saturated component

able values of *V*, *b* and *N* are listed in Table 2 for both the Na I and Ca II spectral lines.

shown superposed on the observed line-profiles in Figures 2 and 3.

Our profile fits have been performed using the *minimum* number of absorption components, and when more than one line of a species is available (such as the Na I doublet), both profiles are fit simultaneously. We have used the criterion of Vallerga et al. (1993) such that the addition of extra components (which will always improve the fit at some level) results in a reduction of the chi-squared residual error between the observed and computed data points of < 1%. Errors for the derived component column densities (for unsaturated components) are also listed in Table 2. All of these model fits are

The far-UV spectra were searched for interstellar absorption lines that possessed IV features with velocities consistent with those found from previous studies of both stars using the *I.U.E.* satellite (PGB81, PG83). These IV components (occurring at *V* ~ +90 km s⁻¹ for HD 37 318, and *V* ~ -60 km s⁻¹ for HD 36 665) were then fitted and analyzed using the same techniques as outlined above for the visible interstellar lines. We note that only for the case of the O VI (λ1031.9Å) interstellar line was continuum placement judged to be problematic, due to the presence of nearby O VI stellar and molecular H₂ line features. Our final choice of continuum placement for the two

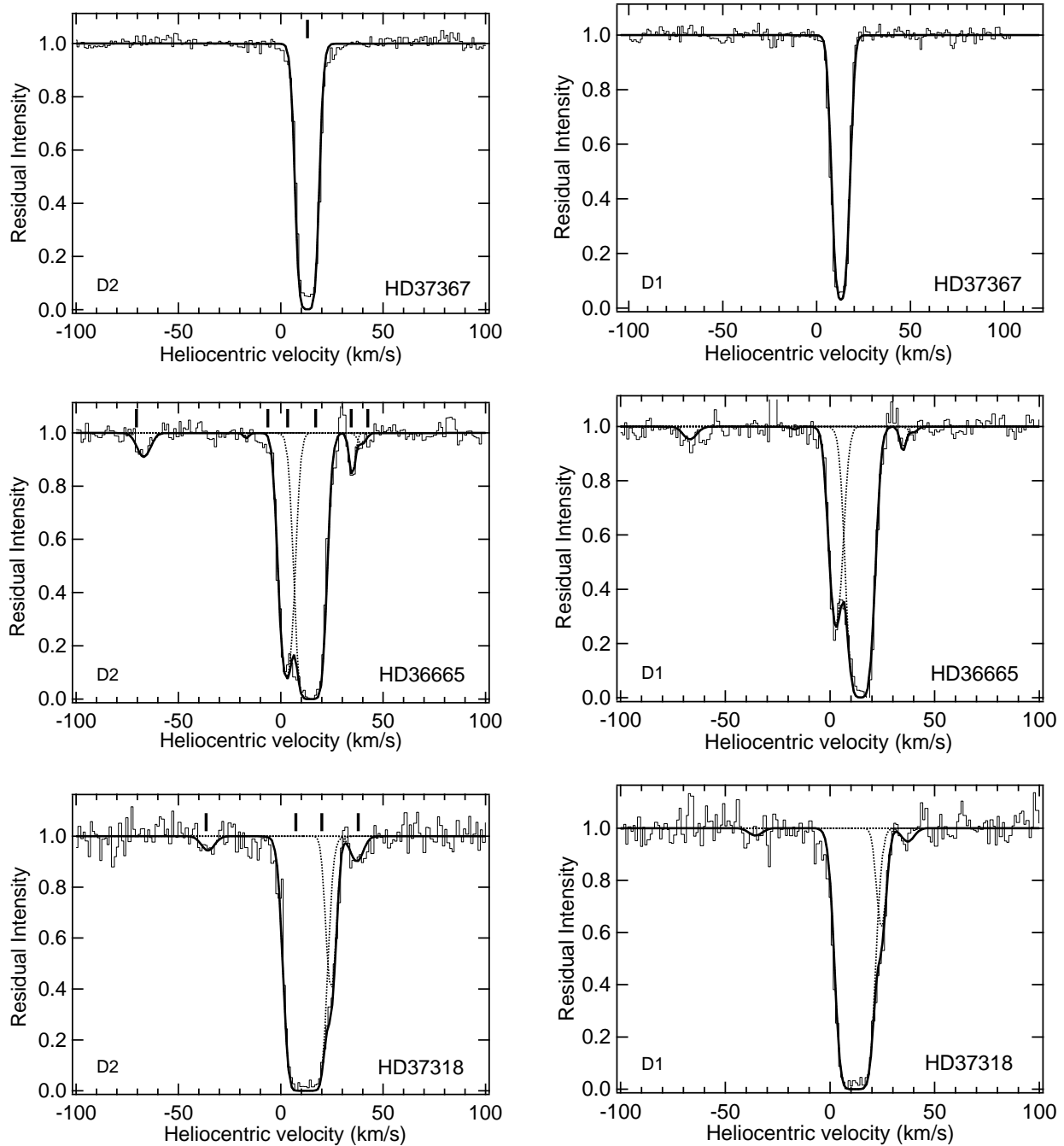


Fig. 2. Interstellar Na I D2 and D1 absorption lines observed towards the 3 stars in line-of-sight towards the S147 SNR. Superposed on the residual intensity data points (light full line) is the multi-component best-fit absorption model (see Table 2). The dotted lines indicate each of the components used in the model fits.

stars was guided by the examples given in Lehner et al. (2001). It was found that the absorption centered at ~ -60 km s $^{-1}$, detected in 5 of the far-UV lines seen towards HD 36 665, was best fit using a two-component model (with cloud components at $V = -64$ and -52 km s $^{-1}$). Absorption components with a similar velocity-split were also observed in the Ca II spectrum of this sight-line. The high-ionization line of O VI ($\lambda 1031.9\text{\AA}$) was strongly detected towards both stellar targets, but no IV features with velocities in common with those detected in the

lower ionization UV lines were seen. However, a partially resolved absorption feature was observed at $V \sim +40$ km s $^{-1}$ in the O VI lines towards both stars and this component was fitted in tandem with the strong central absorbing component. Components with a similar velocity ($\sim +40$ km s $^{-1}$) were also detected in the Na I and Ca II lines. All of the far-UV absorption lines possessing these intermediate-velocity features and their associated model fits are shown in Figures 4 and 5, and the best-fit UV absorption-line parameters are listed in Table 3.

The best-fit b -values for the UV lines are generally large, indicating the presence of absorption structure that is unresolved by the *FUSE* instrument.

We also note that the *FUSE* spectra of both HD 36 665 and HD 37 318 contain many (strong) molecular H_2 lines associated with the Lyman (B-X) and Werner (C-X) bands. None of these lines is accompanied by an absorption component with a velocity consistent with the IV features detected by the atomic lines. Similarly, Gondhalekar & Phillips (1980) also failed to detect high-velocity components in the many ultraviolet $^{12}C^{16}O$ lines observed towards HD 36 665. This is in marked contrast to the Monoceros Loop SNR in which IV molecular H_2 was observed at $V = +65 \text{ km s}^{-1}$ in six of the $J = 3$ rotational levels (Welsh et al. 2002a).

4. Discussion

It is immediately apparent from Figures 2 and 3 that the $Na\ I$ and $Ca\ II$ absorption profiles recorded towards both HD 36 665 and HD 37 318 are far more complex and span a much wider range in velocity than the profiles recorded towards HD 37 367. Since this latter star lies in the same sight-line as S147, but is $\sim 500\text{pc}$ foreground to the nominal distance to the remnant, we can confidently assign the additional higher-velocity absorption components observed towards both HD 36 665 and HD 37 318 as being due to the interaction of the expanding SNR with the surrounding ISM. Our following discussion will focus on the absorption properties of these intermediate-velocity (IV) interstellar components.

4.1. The $Na\ I$ D-line absorption spectra

In Figure 2 we see that all 3 stars show strong central absorption over the velocity range of -10 to $+30 \text{ km s}^{-1}$, which we associate with absorption due to the foreground line-of-sight interstellar medium towards these targets. From these data we assign velocities of $V = +13.5$, $V = +14.5$ and $V = +12.0 \text{ km s}^{-1}$ to the main (line-of-sight) absorption towards HD 37 367, HD 36 665 and HD 37 318 respectively. The absorption component observed towards HD 36 665 at $V \sim 0 \text{ km s}^{-1}$ is seen to be partially resolved in our spectra. This component becomes stronger and more saturated in the spectrum of HD 37 318, which is consistent with the greater distance of the ISM being sampled.

The higher-velocity components observed in the $Na\ I$ spectra at $V = -67$ and $+39 \text{ km s}^{-1}$ towards HD 36 665 and at $V = -35 \text{ km s}^{-1}$ towards HD 37 318 presumably originate in the disturbed ISM surrounding the S147 SNR. These absorption components were also detected at similar velocities in the $Ca\ II$ spectra, and confirm the original observations of Silk & Wallerstein (1973) who first detected IV gas towards HD 36 665 at $V_{helio} = -58 \text{ km s}^{-1}$. Our observations are also consistent with the $H-\alpha$, $N\ II$ and $S\ II$ emission line observations of S147 by Kirshner & Arnold (1979) who derived a *systematic* expansion velocity of $\sim 80 \text{ km s}^{-1}$ for the remnant.

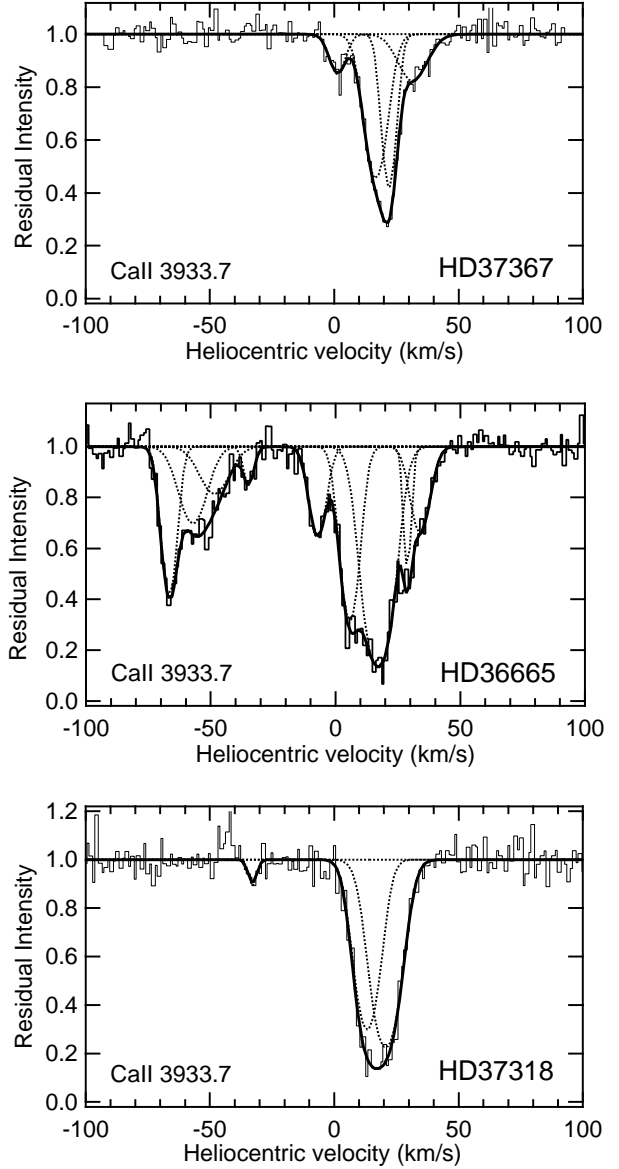


Fig. 3. Observed and best-fit models for the interstellar $Ca\ II$ -K absorption profiles recorded towards the 3 target stars. Symbols are as stated in Figure 2.

4.2. The $Ca\ II$ K-line absorption spectra

The $Ca\ II$ K-line profiles of Figure 3 clearly show that the strong foreground line-of-sight absorption is formed over a similar velocity range to that of the $Na\ I$ spectra (i.e. 0 to $+30 \text{ km s}^{-1}$). Additional, higher-velocity components have been detected at $V = -65.5$, -55.5 , -46.5 and $+37.5 \text{ km s}^{-1}$ towards HD 36 665, indicating that this sight-line is clearly complex and consists of many warmer and/or more ionized fast-moving gas clouds. The sight-line towards HD 37 318 is far less complicated with the strong central $Ca\ II$ absorption being accompanied by a single extra low-velocity component at $V = -33.0 \text{ km s}^{-1}$. Figure 3 clearly shows no sign of the component detected at $V = +90 \text{ km s}^{-1}$ in the *I.U.E.* data of PG83. Since this IV absorption

component was not detected in either Na I or Ca II towards HD 37318, it must contain mainly ionized (and warmer) gas.

All these data are consistent with observations towards other SNRs such as the Monoceros Loop, the Vela SNR and IC 443, in that the visible absorption profiles possess a multi-component structure indicative of sight-lines that pass through a highly disturbed and/or inhomogeneous interstellar medium. The various absorption components can be identified with expanding gas shells and/or disrupted ambient clouds of gas. The physical complexity of these disrupted interstellar clouds can be easily seen in the many contorted filaments of gas emission shown in Figure 1, which suggests a chaotic pattern of disruption of the surrounding ISM. In the following sections we will attempt to describe the physical and chemical nature of these disturbed interstellar regions.

4.3. The Na I/Ca II ratios

The column-density ratio of $N(\text{Na I})/N(\text{Ca II})$ has been widely used as a diagnostic of the physical state of gas clouds in the interstellar medium (Routly and Spitzer 1952). For low-velocity clouds a ratio of > 1.0 is generally found in the ISM. Our data show similar ratios for the strong central foreground absorption components observed towards all 3 stars. In contrast, interstellar shocks produced by fast-moving gas clouds can cause thermal sputtering and collisions of interstellar dust grains, which then return Ca into the gas phase, resulting in a low observed value ($\ll 1.0$) of the Na I/Ca II ratio. For the (well-resolved) IV components at $V = -65$ and $+39 \text{ km s}^{-1}$ seen towards HD 36665 we obtain Na I/Ca II ratios of 0.085 and 0.054 respectively. Similarly low values of this ratio have been found for the Vela SNR by Danks & Sembach (1995), in which SN-driven shocks were forwarded to explain the anomalous (i.e. near-solar) gas-phase abundance ratio of $[\text{Na}/\text{Ca}]$ in the high-velocity gas cloud components. However, we note that the Na I/Ca II ratio can also reflect the unusual ionization of Na and Ca due to a nearby strong source of UV photon flux. We shall comment further on this possibility in the following discussion of the UV absorption properties of the IV gas components observed towards S147.

4.4. The far-UV absorption spectra

As shown in Figure 4 our *FUSE* observations have revealed partially resolved intermediate-velocity absorption features at $V = -64$ and -52 km s^{-1} towards HD 36665 in the UV lines of Fe II, N I and O I, in addition to a strong blended component at $V = -53 \text{ km s}^{-1}$ in the N II line at 1084.0\AA . Absorption components with a similar velocity were also detected in our visible absorption spectra towards HD 36665, and by PGB81 in the near-UV lines of Fe II, Mg I, Mg II, Al II, C II and Si II. All these observations indicate that the gas travelling with these velocities is not only composed of neutral components (e.g. Na I, Mg I and O I), but it must also contain significant amounts of warmer and more ionized components due to the detection of Fe II, Al II and N II. Given the very similar velocities of these IV components it seems likely that the neutral and ionized gas may be in

the form of co-moving sheets or shells of interstellar material that have been disrupted by the expansion of the SNR.

In the case of the sight-line towards HD 37318 we note that the IV feature was detected only in the far-UV lines of Fe II and N II at $+92 \text{ km s}^{-1}$. It was present neither in the Na I or Ca II lines, nor in any of the low-ionization far-UV lines. These results are consistent with the near-UV observations of this sight-line by PG83 in which this IV component was detected only in the lines of C II, Mg II, Al II, Al III, Si II, S II and Fe II. All these data strongly suggest that this component is *not* composed of appreciable amounts of cold and neutral gas, but instead is mainly composed of (warmer) ionized gas. We note that the distance to HD 37318 ($\sim 1380\text{pc}$) suggests that the sight-line samples both the near and far sides of the remnant. This view is strongly supported by the detection of the $+92 \text{ km s}^{-1}$ component which is most probably associated with gas receding away from the SNR. We might also have expected to detect approaching (negative-velocity) IV gas along this sight-line. Its non-detection towards a star of this distance (which lies well beyond the nominal distance to the SNR) may well be due to large-scale density inhomogeneities in the near-side filamentary shell(s) of the SNR. Similar behavior has been observed towards many stars with sight-lines towards the Vela SNR, in which maps of the observed high velocity components revealed a chaotic structure of kinematic motions (due to interactions with pre-existing ambient interstellar clouds), rather than a picture of coherent expansion of the remnant material (Jenkins et al. 1984).

Highly ionized O VI ($\lambda 1032\text{\AA}$) gas components with a velocity of $V \sim +40 \text{ km s}^{-1}$ have been detected along both stellar sight-lines. This high-temperature gas cloud could be foreground to the SNR, but its anomalously high velocity compared with gas found in the general ISM suggests that it is more probably associated with the expansion of the SNR. We note that no IV components were detected in the high ions of C IV, Si IV or N V towards both stars by PGB81 and PG83. Using their published upper limit for intermediate velocity C IV absorption towards HD 37318 of $\log N(\text{C IV}) < 12.96 \text{ cm}^{-2}$, we obtain a ratio of $N(\text{C IV})/N(\text{O VI}) < 0.27$. This ratio only has physical significance if the C IV and O VI coexist in the same absorbing cloud, and we note that the published upper limit for C IV was determined for absorption at $V = +90 \text{ km s}^{-1}$ by PG83. However, if we assume that the two species do physically coexist then this ratio is consistent with that observed in the hot gas of the galactic disk (Spitzer 1996). The ratio is also consistent with that derived for hot gas in the evolved supernova bubble model of Slavin & Cox (1992) in which an isolated SN event explodes into interstellar gas with an ambient density of $0.1 - 0.3 \text{ cm}^{-3}$ and a magnetic field of $1 - 3 \mu\text{G}$. Therefore, at present we cannot confirm where the $V = +40 \text{ km s}^{-1}$ O VI absorption is taking place. However we do note two things: (i) the observed $N(\text{C IV})/N(\text{O VI})$ ratio is not consistent with that derived for models that involve turbulent mixing layers, and (ii) the H- α emission from S147 has been reported by Kirshner & Arnold (1979) at a similar velocity to that of the O VI absorption.

Clearly the gas surrounding S147 has been highly disrupted by the initial SN explosion, and thus it is of great interest to investigate how the passage of fast-moving interstellar shocks

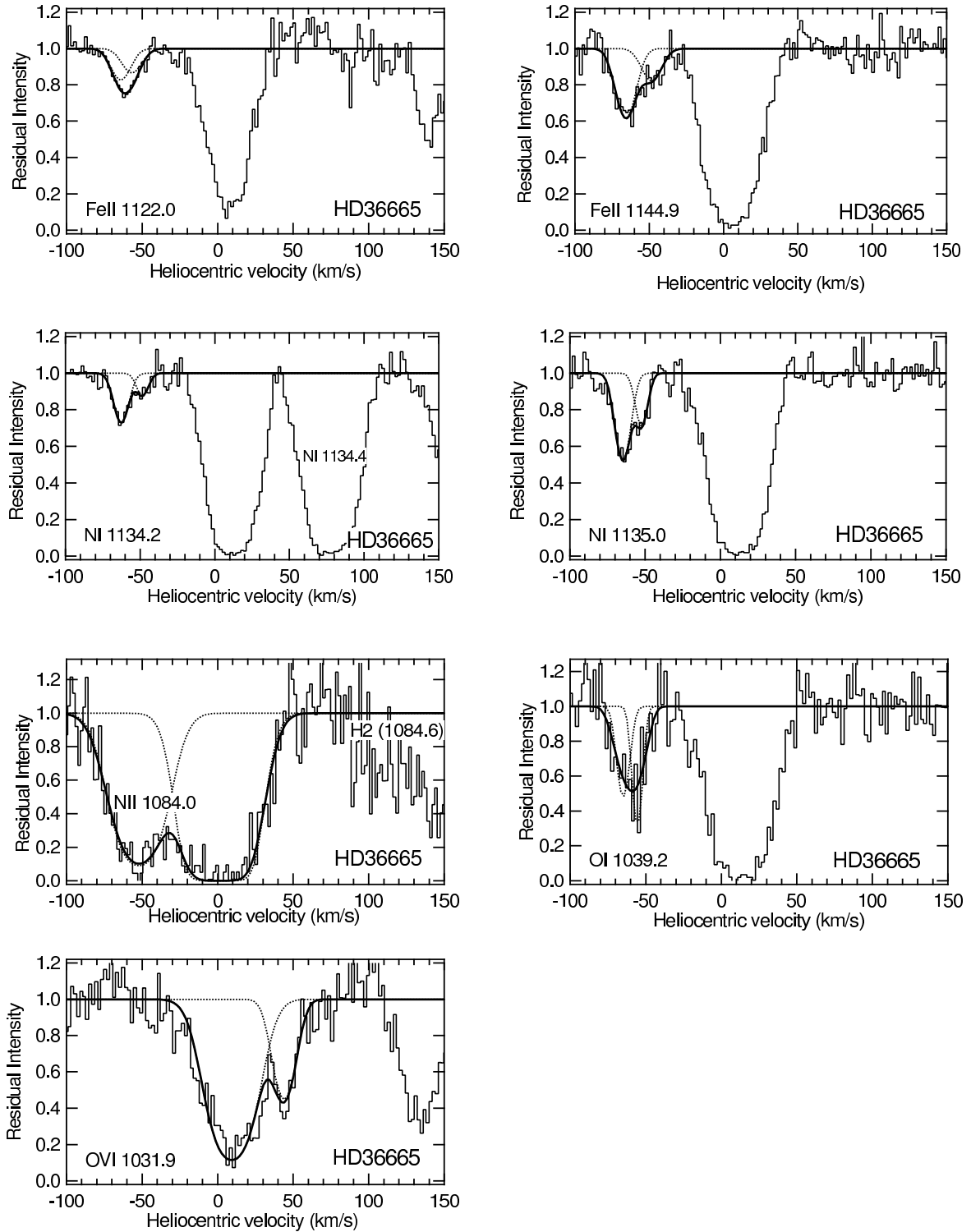


Fig. 4. Observed and best-fit models for the high-velocity absorption features recorded in the far-UV lines towards the star

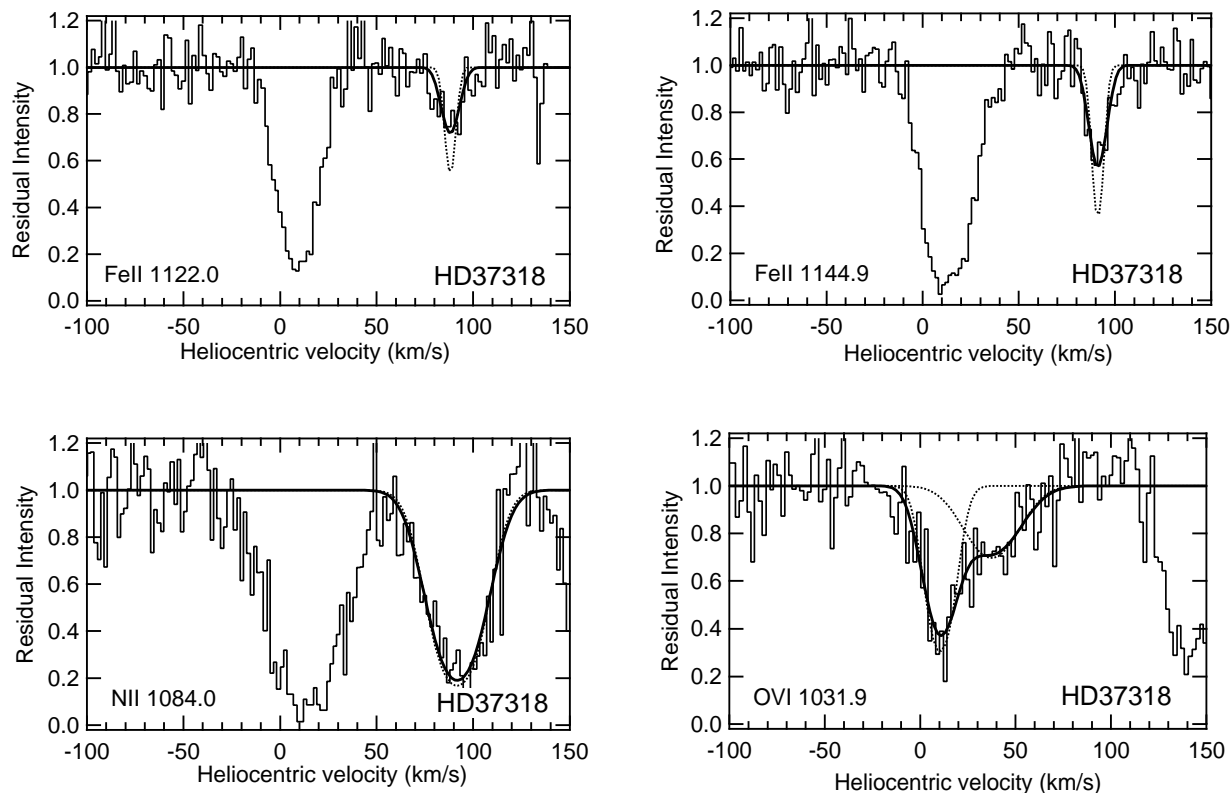


Fig. 5. Observed and best-fit models for the high-velocity absorption features recorded in the far-UV lines towards the star HD37318.

and the influence of local ionization processes on the ambient interstellar gas and dust may have altered their gas-phase element abundances. Previous studies of high-velocity gas clouds associated with SNRs have revealed an increase in the relative abundances of Fe, Si and Al compared with their cosmic values, while elements such as N, O and Ar have shown an opposite behavior (Savage & Sembach 1996; Jenkins et al. 1984; Welsh et al. 2001).

The interstellar abundance of a given element, X, relative to that of hydrogen (H) is normally defined as $[N(X)/N(H)]_{cloud}$, where $N(X)$ and $N(H)$ are the total column densities of the elements X and H present in the gas cloud. For many elements (except N) the greatest column-density contribution arises in absorption lines of their first and second ionization states, which are observable at ultraviolet wavelengths. These observed values can then be compared to their solar (cosmic) abundance values (as listed in Table 5 of Savage & Sembach 1996), such that an elemental depletion or over-abundance can be determined for the gas cloud under investigation. Unfortunately direct measurement of the hydrogen column density for the IV clouds observed towards both sightlines associated with S147 are unavailable. This is also the case for the element sulfur which, because it is normally assumed to be undepleted in the general ISM, has been widely used as a surrogate abundance comparison element. We have therefore decided to use comparisons of the ratios of the actual measured element column densities of the IV clouds (listed in Tables 2 and 3) as a potential probe of the variation of element abundance. We have al-

ready discussed how the variation of the $N(\text{Na I})/N(\text{Ca II})$ cloud column-density ratio can be used as an interstellar gas diagnostic in Section 4.3, and the column-density comparison method for UV absorption lines has also been used successfully by Jenkins et al. (1984) and Trapero et al. (1996) for high-velocity gas clouds in the ISM.

4.5. Element abundances in the IV gas

In the following analysis we use the *total* column-density value for the summed $V = -65$ and -56 km s^{-1} components for the various lines of each element detected towards HD 36665, as listed in Table 3. For Na and Ca, we use the column-density values for the -65 km s^{-1} component, as listed in Table 2. For the HD 37318 sight-line we use the corresponding $V = +92 \text{ km s}^{-1}$ component column-density values. We have also supplemented these N I, N II, O I, Fe II, Na I and Ca II data with the column-density values for Mg I, Mg II, Al II, and Si II listed by PGB81 and PG83 to derive the ratios of $[\text{Mg}/\text{Fe}]$, $[\text{Al}/\text{Si}]$, $[\text{Si}/\text{Fe}]$, $[\text{N}/\text{Fe}]$, $[\text{O}/\text{Fe}]$ and $[\text{Na}/\text{Ca}]$ listed in Table 4 for the intermediate-velocity components observed towards HD 36665 and HD 37318. Note that these ratios include only the ionization stages mentioned above. If ionization is important, a significant amount of each element may be in higher ionization stages. For comparison purposes we also present values of these element column-density ratios for fast-moving interstellar gas clouds observed at $V = +65 \text{ km s}^{-1}$ towards HD 47240 in the Monoceros Loop SNR (Welsh et al. 2001), at $V =$

Table 4. Element column-density ratios in SNR intermediate-velocity gas compared with cold, diffuse ISM gas and cosmic abundances

Element Ratio	Ionization Stages (SNRs)	S147 HD36 665	S147 HD37 318	Monoceros Loop	Vela SNR	ζ Oph	Cosmic Ratio
Mg/Fe	(Mg I + Mg II)/Fe II	0.88	0.5	>1.92	0.71	35.7	1.18
Al/Si	Al II/Si II	0.045	0.15	0.028	0.071	0.007	0.085
Si/Fe	Si II/Fe II	1.91	1.07	2.63	2.24	3.5	0.72
N/Fe	(N I + N II)/Fe II	6.1	3.88	2.79	N/A	575	2.88
O/Fe	O I/Fe II	10.7	<1.09	12.9	11.2	2240	22.9
Na/Ca	Na I/Ca II	0.085	N/A	1.14	N/A	166	0.93

-58 km s⁻¹ towards HD 72089 in the Vela SNR (Jenkins et al. 1998, Jenkins & Wallerstein 1996) and in the cold and diffuse gas at $V = -15$ km s⁻¹ observed towards ζ Oph by Savage et al. (1992) and Morton (1975). All these ratios are compared with the ratios of their canonical cosmic abundances (relative to that of the Sun) as listed by Savage & Sembach (1996).

Inspection of Table 4 reveals that the column-density ratios obtained for IV gas in SNRs are generally quite different from the values obtained for cold and diffuse gas of the ISM as observed towards ζ Oph. Clearly the physical and chemical conditions in the disrupted gas associated with SNRs are different to those normally encountered in slow-moving gas of the general ISM. Several authors have found that the refractory elements of Fe, Ca, Mg, Al, C and Si are not heavily depleted in IV interstellar gas clouds, a result which is easily explained by invoking interstellar dust grain destruction mechanisms (such as thermal sputtering and grain-grain collisions) that operate within fast-moving gas clouds and return these elements back into the gas phase (Barlow 1978). Therefore we might expect the [Mg/Fe] and [Al/Si] ratios in disrupted gas to have column-density ratios similar to their respective solar abundance ratio values of 1.18 and 0.085. For the 4 SNR sight-lines sampled, the measured values suggest that this is indeed the case. We note, however, that as mentioned in Section 4.3 the Na I/Ca II ratio can be also affected by local ionization processes, and our UV absorption data taken towards HD 36 665 in S147 have shown that the IV component is composed of both neutral and ionized gas. The doppler b -values derived from the Na I and Ca II intermediate-velocity components for this sight-line (listed in Table 2) also suggest the presence of high-temperature or highly turbulent gas in this particular IV cloud. Therefore, grain destruction by fast-moving shocks may not be the sole process responsible for the level of depletion of Ca revealed by our data.

We note that the [N/Fe] ratios for both S147 sight-lines are a factor of 1.3 to 2.1 larger than the cosmic ratio, whereas [O/Fe] is smaller by a factor of 2 to 20. We have inspected the *FUSE* spectral data in the low S/N channels of SiC2a and SiC1b recorded towards both HD 36 665 and HD 37 318 and have found a strong absorption feature centered at 989.8Å that extends over a velocity range of ± 100 km s⁻¹ in both sight-lines. Inspection of the atomic line list by Morton (2003) reveals the presence of the strong ground-state line of N III at 989.799Å. Unfortunately this line is blended with the strong interstellar line of Si II at 989.87Å and hence it is impossible for us to assess the column density contribution of N III in either

sight-line. However, it is clear that the *total* column density of $N(N I + N II + N III)$ can only be higher than the one used in deriving the observed [N/Fe] ratios. In addition, the N lines may be saturated, which would create a tendency to *underestimate* the N column density. Thus these ratios for the S147 sight-lines in Table 4 must really represent lower limit values. The apparent deficiency of O with respect to Fe can be attributed to ionization effects, in that radiation from shock fronts in these disturbed regions photo-ionizes atoms to higher ion states that are generally unobservable (Jenkins et al. 1998). For the case of O, the inability to observe the contribution of interstellar O II to the total sight-line column density (of neutral and ionized gas) has been estimated from standard photo-ionization models to be up to ~ 0.2 dex by Cardelli et al. (1995) and Sembach & Savage (1996). Thus, this missing O II will increase the ratio values for [O/Fe] listed in Table 4, such that the overall depletion level of oxygen towards S147 is probably small. Thus in summary, although the lack of knowledge of the column density of hydrogen in the IV gas clouds seen towards S147 precludes us from deriving absolute values for element depletion and abundances, our measured column-density ratios suggest that the refractory elements (such as Fe, Si and Mg) are present in near-solar abundance ratios, while N and O are not heavily depleted, and that N may in fact be slightly overabundant. Such results are consistent with abundance studies of gas associated with other SNRs.

5. Conclusion

We have obtained high-resolution (3 km s⁻¹) spectra of the interstellar Na I and Ca II absorption lines observed towards 3 stars with distances ranging from 360 - 1380pc in sight-lines towards the Shajn 147 SNR. The two most distant stars, HD 36 665 ($d = 880$ pc) and HD 37 318 ($d = 1380$ pc), lie beyond the SNR gas and possess complex absorption profiles in which components have been detected over a velocity range of -65 to + 80 km s⁻¹. The foreground star, HD 37 367, exhibits none of these intermediate velocity (IV) components. We have fit all the absorption components observed in the Na I and Ca II lines towards the 3 stars with models of cloud-component velocity, doppler broadening and column density. For the well resolved IV components at $V_{helio} = -65$ and +39 km s⁻¹ observed towards HD 36 665 we have obtained $N(Na I)/N(Ca II)$ column-density ratios of 0.085 and 0.054 respectively. Such low ratio values can be best explained by the influence of shocks and ionization on the disturbed SNR gas clouds.

We have also obtained far-UV absorption spectra along the sight-lines to HD 36 665 and HD 37 318 using the NASA *FUSE* satellite. These observations have revealed IV features at velocities of -65 and -52 km s $^{-1}$ in the interstellar absorption lines of N I, N II, O I and Fe II seen towards HD 36 665. Based on the detection of Na I and Ca II components at these velocities, this IV cloud is probably composed of both neutral and ionized gas shells. For the case of the 1380pc sight-line to HD 37 318, IV gas was only detected in the UV lines of Fe II and N II at $V = +90$ km s $^{-1}$, suggesting that this outwardly moving cloud is composed mainly of warm and ionized gas. The inability to detect IV components with negative velocities towards this star (which resides beyond the Shajn 147 SNR), suggests that the velocity structure of the expansion of the SNR is not coherent and that randomly distributed large-scale inhomogeneities must exist throughout the ambient interstellar clouds.

Highly ionized gas has been detected at $V \sim +40$ km s $^{-1}$ in the lines of O VI λ 1032Å along the sight-lines to both stars. The column-density ratio of N(C IV)/N(O VI) < 0.27 is consistent with that predicted for an evolved supernova by Slavin & Cox (1992). However, this ratio is also similar to that observed in many sight-lines passing through hot gas in the general ISM (Spitzer 1996). Therefore, we are unable to definitely associate this high-ion absorption with gas in Shajn 147.

We have derived estimates of the observed column-density ratios of [Mg/Fe], [Al/Si], [Si/Fe], [N/Fe], [O/Fe] and [Na/Ca] for the intermediate-velocity clouds seen in the sight-lines towards Shajn 147 and also towards fast-moving gas in the Monoceros Loop and Vela SNRs. The ratios for IV gas clouds in all these SNRs are generally quite different from those values seen in the diffuse and cold ISM. Such differences are almost certainly due to the destruction of interstellar dust grains in these highly disturbed regions that returns elements back into the gas phase. For the refractory elements of Fe, Si, Al and Mg we observe a column-density ratio pattern that is similar to that derived for undepleted (solar abundance) gas. The elements of N and O are greatly influenced by the ionization conditions in these regions, and when the column-density contribution from the unobserved species of N III and O II are accounted for, it appears that neither N nor O are significantly depleted.

Acknowledgements. We are grateful to the staff and directorate of the Observatoire de Haute Provence (France) for the ground-based observations. We would also like to recognize members of the *FUSE* project team at Johns Hopkins University. Financial support for both BYW and SS came from Guest Investigator funding from the NASA *FUSE* project under contract NAS5-32985 to the Johns Hopkins University.

References

- Barlow, M. 1978, MNRAS, 183, 367
 Cardelli, J., Sembach, K. & Savage, B., 1995, ApJ, 440, 241
 Chevalier, R., 1974, ApJ, 188, 501
 Chevalier, R., 1999, ApJ, 511, 798
 Cioffi, D., McKee, C. & Bertschinger, E., 1988, ApJ, 334, 252
 Danks, A. & Sembach, K., 1995, AJ, 109, 2627
 ESA, 1997, The Hipparcos Satellite Catalogue, ESA SP-1200
 Furst, E. & Reich, W., 1986, A&A, 163, 185
 Gondhalekar, P. & Phillips, A.P., 1980, MNRAS, 191, 13
 Halbedel, E., 1996, PASP, 108, 833
 Jenkins, E., Silk, J. & Wallerstein, G., 1976, ApJS, 32, 681
 Jenkins, E., Wallerstein, G. & Silk, J., 1984, ApJ, 278, 649
 Jenkins, E. & Wallerstein, G., 1996, ApJ, 462, 758
 Jenkins, E., Tripp, T., Fitzpatrick, E. et al., 1998, ApJ, 492, L147
 Kirshner, R. & Arnold, C., 1979, ApJ, 229, 147
 Kundu, M., Angerhofer, P., Furst, E. & Hirth, W., 1980, A&A, 92, 225
 Lallement, R., Bertin, P., Chassefiere, E. & Scott, N., 1993, A&A, 271, 734
 Lehner, N., Fullerton, A.W., Sembach, K.R. et al., 2001, ApJ, 556, L103
 Meyer, D., Jura, M. & Cardelli, J., 1998, ApJ, 493, 222
 Minkowski, R., 1958, Rev. Mod. Phys., 30, 1048
 Moos, H.W., Cash, W., Cowie, L. et al., 2000, ApJ, 538, L1
 Morton, D.C., 1975, ApJ, 197, 85
 Morton, D.C., 2003, ApJS, 149, 205
 Phillips, A., Gondhalekar, P. & Blades, C., 1981, MNRAS, 195, 485 (PGB81)
 Phillips, A. & Gondhalekar, P., 1983, MNRAS, 202, 483 (PG83)
 Routly, P. & Spitzer, L., 1952, ApJ, 115, 227
 Sahnou, D., Moos, H., Ake, T. et al., 2000, ApJ, 538, L7
 Sankrit, R. & Blair, W., 2002, ApJ, 565, 297
 Sankrit, R., Blair, W. & Raymond, J.C., 2003, ApJ, 589, 242
 Sauvageot, J., Ballet, J. & Rothenflug, R., 1990, A&A, 227, 183
 Savage, B., Massa, D., Meade, M. & Wesselius, P., 1985, ApJS, 59, 397
 Savage, B., Cardelli, J. & Sofia, U., 1992, ApJ, 401, 706
 Savage, B. & Sembach, K., 1996, ARA&A, 34, 279
 Sembach, K. & Savage, B., 1996, ApJ, 457, 211
 Sfeir, D., Lallement, R., Crifo, F. & Welsh, B.Y., 1999, A&A, 346, 785
 Silk, J. & Wallerstein, G., 1973, ApJ, 181, 799
 Siluk, R. & Silk, J., 1974, ApJ, 192, 51
 Slavin, J. & Cox, D., 1992, ApJ, 392, 131
 Sofia, U., Cardelli, J. & Savage, B., 1994, ApJ, 430, 650
 Spitzer, L., 1996, ApJL, 458, L29
 Trapero, J., Welty, D.E., Hobbs, L.M. et al., 1996, ApJ, 468, 290
 Vallerger, J.V., Vedder, P., Craig, N. & Welsh, B.Y., 1993, ApJ, 411, 729
 Welsh, B.Y., Vedder, P. & Vallerger, J.V., 1990, ApJ, 358, 473
 Welsh, B.Y., Sfeir, D., Sallmen, S. & Lallement, R., 2001, A&A, 372, 516
 Welsh, B.Y., Rachford, B. & Tumlinson, J., 2002a, A&A, 381, 566
 Welsh, B.Y., Sallmen, S., Sfeir, D. & Lallement, R., 2002b, A&A, 391, 705
 Welsh, B.Y., Sallmen, S., Jelinsky, S. & Lallement, R., 2003a, A&A, 403, 605
 Welsh, B.Y. & Sallmen, S., 2003b, A&A, 408, 545

Barlow, M. 1978, MNRAS, 183, 367

Cardelli, J., Sembach, K. & Savage, B., 1995, ApJ, 440, 241

Chevalier, R., 1974, ApJ, 188, 501

Chevalier, R., 1999, ApJ, 511, 798

Cioffi, D., McKee, C. & Bertschinger, E., 1988, ApJ, 334, 252

Danks, A. & Sembach, K., 1995, AJ, 109, 2627

ESA, 1997, The Hipparcos Satellite Catalogue, ESA SP-1200

Furst, E. & Reich, W., 1986, A&A, 163, 185

Gondhalekar, P. & Phillips, A.P., 1980, MNRAS, 191, 13